ACS APPLIED MATERIALS & INTERFACES

www.acsami.org

Research Article

Highly Sensitive Photopolymer for Holographic Data Storage Containing Methacryl Polyhedral Oligomeric Silsesquioxane

Po Hu, Jinhong Li, Junchao Jin, Xiao Lin, and Xiaodi Tan*

Cite This: *ACS Appl. Mater. Interfaces* 2022, 14, 21544−21554

Read Online

ACCESS | Metrics & More | Article Recommendations | Supporting Information

ABSTRACT: Herein, via introducing eight methacryl polyhedral oligomeric silsesquioxane (Ma-POSS), we dramatically enhance the holographic performance of phenanthraquinone-doped poly(methyl methacrylate) (PQ/PMMA) photopolymer with excellent characteristics of high sensitivity, high diffraction efficiency, and neglectable volume shrinkage for holographic data storage, the photosensitivity, diffraction efficiency, and volume shrinkage reaching 1.47 cm/J, ∼75%, and ∼0.09%, respectively. Ma-POSS here dramatically enhances the photosensitivity ∼5.5 times, diffraction efficiency more than 50%, and suppressed the volume shrinkage over 4 times. Further analysis reveals that Ma-POSS obviously increased the molecular weight by grafting PMMA to be a star-shaped macromolecule. And the residual C═C of POSS−PMMA dramatically increased the photosensitivity. Moreover, the star-shaped POSS−PMMA acting as a plasticizer dramatically enhances the mechanical properties and so reduces the photoinduced volume shrinkage of PQ/PMMA. Finally, by the use of the POSS−PMMA/PQ in a collinear holography system, it appeared to be promising for a fast but low bit error rate in holographic information storage. The current study thence has not only successfully synthesized photopolymer materials with potential for highly sensitive holographic storage applications but also investigated the microphysical mechanism of the impact of Ma-POSS on the holographic properties of PQ/PMMA photopolymer and clarified the thermal- and photoreaction processes of the POSS−PMMA/PQ photopolymer.

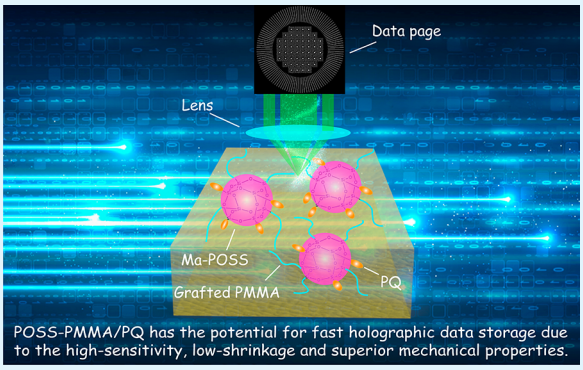

KEYWORDS: *photopolymer, star-shaped macromolecular, high-sensitive, Ma-POSS, holographic data storage*

INTRODUCTION

The exponential growth of data in the era of information and Internet, in which the global scope of the datasphere will shoot up from 33 ZB in 2018 to 175 ZB in 2025 (IDC report 2020),[1] poses severe challenges for existing data storage systems,[2−4] even though not all data are worth storing. Because data is a vital resource and support in accomplishing artificial intelligence and big data applications,[5−7] the development of low-cost and convenient data storage technology is undoubtedly a benefit that will promote people to enter an even more data-driven future.[8−10] Nevertheless, green characteristics of optical data storage urge scientists to utilize new technologies and novel functional materials to break the storage-capacity limit of the optical disc and cope with the explosive demand for data storage. Multidimensional optical data storage technologies,[2,11,12] through multiplexing new physical dimensions including polarization,[13−16] wavelength,[13,17] intensity, and florescence[13,18] in various materials, for example, quartz glass,[19,20] silver clusters embedded in glass, and gold or silver nanoparticles,[11−13,16,18,21] provide a novel and reliable approach for ultrasecure optical encryption and high-capacity data storage.

Volume holographic data storage,[22−26] utilizing multiple coherent laser beams to record the information onto photorefractive materials, is also recognized as a promising new generation of optical data storage technology with a huge capacity and high write/read speed, and it is economically sustainable. A lack of appropriate storage medium, however, remains a major obstacle to volume holographic storage achieving its full practical application potential.[27,28] On the one hand, the troublesome intrinsic defects of volume shrinkage, poor oxygen resistance, and thin thickness have severely inhibited the feasibility of most existing photopolymer functional materials in photolithography for high-density volume holographic data storage.[29−32] On the other hand, the excellent characteristics of low volume shrinkage and high sensitivity facilitate the application of phenanthraquinone-

Received: March 4, 2022
Accepted: April 22, 2022
Published: April 29, 2022

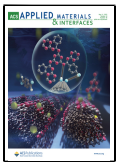

https://doi.org/10.1021/acsami.2c04011
ACS Appl. Mater. Interfaces 2022, 14, 21544−21554

Scheme 1. Schematic Representation of Possible Architecture for Star-Shaped POSS−PMMA Macromolecules

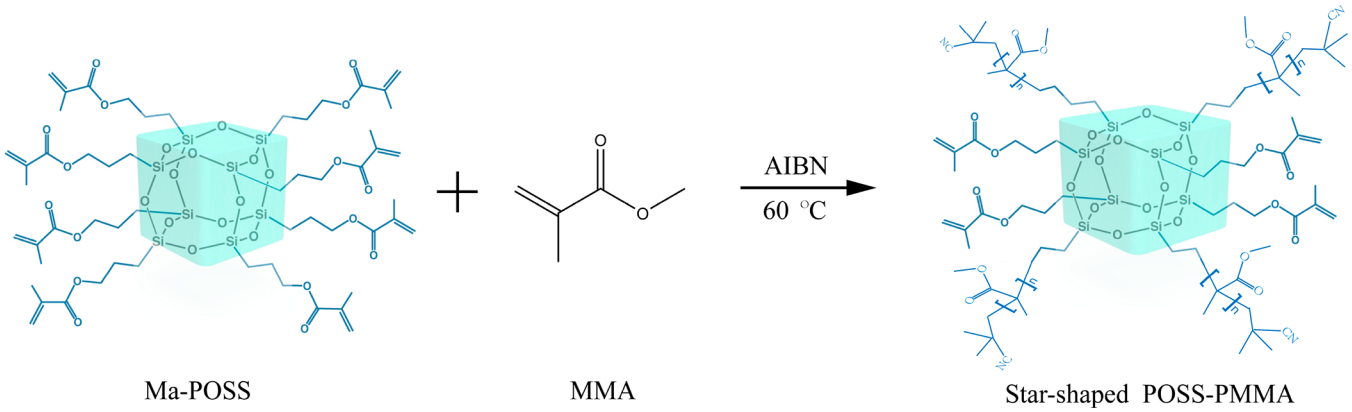

doped poly(methyl methacrylate) (PQ/PMMA) photopolymer in multidimensional holographic storage as a low-cost optical storage medium; however, this photopolymer is itself seriously hampered by its inherent poor holographic performance (e.g., the diffraction efficiency, photosensitivity, refractive index modulation, and so on).[28,33−37] Various strategies have been proposed to optimize the holographic performance of PQ/PMMA photopolymer for volume holography,[27,38,39] with little success. Considering the excellent ultrafast photonic property due to the synergistic effects of the two-dimensional (2D) nanosheet-doped polymer composite (e.g., the Graphdiyne-polymer,[40] MXene-polymer,[41] Tellurium-polymer,[42] Black Phosphorus-polymer,[43] and so on), the nanosheet has the possibility to enhance the photosensitivity of PQ/PMMA, but it is not a good choice due to the poor solubility and dispersity.

As a special family of organic−inorganic hybrid material,[44,45] polyhedral oligomeric silsesquioxane (POSS) $(RSiO_{1.5})_n$ has a cage-shaped core, a rigid, three-dimensional structure, and a switchable branch (such as alkyl, aryl, vinyl, acrylate, epoxide, and so on) at each of the Si sites.[46−48] A benefit to the organic−inorganic structure, POSS shows a huge potential for polymer performance modification according to the high solubility in most organic solutions.[49−53] The POSS-grafting polymers can be prepared by free radical polymerization,[48,54,55] and the method has been used to acquire POSS−PMMA using R-POSS with C═C bond branches during thermal polymerization with methyl methacrylate (MMA).[56−58] The POSS-containing material with star-shaped or network structure in the polymer matrix can dramatically optimize the properties (Scheme 1).[49,53,59−64] Considering our previous report, which shows that photosensitizer PQ can react with the C═C bond of MMA more effectively,[28] the Ma-POSS with eight methacryl (Ma) branches was selected to enhance the holographic performance of the PQ/PMMA photopolymer.

Herein, by introducing Ma-POSS, we significantly enhance the holographic performance of PQ/PMMA photopolymer, in which the diffraction efficiency was successfully enhanced up to ∼75% (increased ∼50% compared with PQ/PMMA) under low-power laser irradiation conditions. More importantly, the photosensitivity hit a new height (first up to 1.47 cm J^{-1}, ∼5.5 times compared with PQ/PMMA) under low-power laser irradiation conditions. The analytical characterization results show that the star-shaped POSS−PMMA acts as a plasticizer that released the polymer matrix, coworking with the residual vinyl on POSS to dramatically enhance the sensitivity during the photoreaction of POSS−PMMA/PQ. At the same time, the star-shaped POSS−PMMA polymer has more excellent mechanical properties (e.g., hardness, elastic modulus, and elastic recovery parameter), and a benefit of these properties is that the photoinduced volume shrinkage of POSS−PMMA/PQ was significantly suppressed over 4 times (from ∼0.4% to ∼0.09%). The collinear holographic information storage and read-out results show that both the bit error ratio (BER) and signal-to-noise ratio (SNR) of POSS−PMMA/PQ are more excellent than those of PQ/PMMA under a low-power short-time storage process. Besides the successful synthesis of POSS−PMMA/PQ photopolymer with potential for holographic storage applications, the current study also clearly elucidates the microphysical mechanism of the effect of Ma-POSS on the high sensitivity and low shrinkage of PQ/PMMA photopolymer and further reveals the mechanism of the thermal- and photopolymerization processes of the POSS−PMMA/PQ photopolymer.

EXPERIMENTAL SECTIONS

Materials. Methyl methacrylate (MMA, 99.5%), photosensitizer phenanthraquinone (PQ, 99.9%), and 2,2-azobis(isobutyronitrile) (AIBN, 99.9%), as a thermo-initiator, were obtained from Shanghai Macklin Co. Ltd. Eight methacryl polyhedral oligomeric silsesquioxane (Ma-POSS) with a purity of 97% was obtained from Hybrid Plastics, Inc. Tetrahydrofuran (THF, analytical reagent (AR)), methanol (AR), and *N*,*N*-dimethylformamide (DMF, AR) were purchased from Shanghai Macklin Co. Ltd. Acetone (AR) and deuterated chloroform ($CDCl_3$, 99.8% for ^{13}C NMR spectroscopy characterization) were purchased from Sinopharm Chemical Reagent Co. Ltd.

Sample Preparation. Proportional amounts of Ma-POSS and MMA monomers, initially, were added into a 30 mL transparent vial, as demonstrated in Figure S1. The workflow and experimental parameters of the photopolymer fabrication were mainly referred to previous research work[28,37,65] and further optimized in the current study. In addition, to evaluate the impact of POSS upon the macrophysical properties of PQ/PMMA photopolymers, composites with different Ma-POSS weight concentrations compared to total monomers (POSS + MMA), such as 5, 10, 15, and 20 wt %, were prepared. PQ photosensitizer 1.0 wt % and AIBN thermo-initiator 1.0 wt % were then added, and the mixtures were sonicated in a water bath at 333 K for 20 min to mix the components thoroughly. The proportion of each component in the mixture in the current study was maintained as (POSS+MMA)/AIBN/PQ = 100:1:1. In the stirring prepolymerization stage, a well-mixed transparent mixture was stirred with magnetic stirrers at 333 K for half an hour, until the composites changed from a solution to a viscous state.[28] The prepolymerized composites were injected into a mold, to form a photopolymer with a

https://doi.org/10.1021/acsami.2c04011
ACS Appl. Mater. Interfaces 2022, 14, 21544−21554

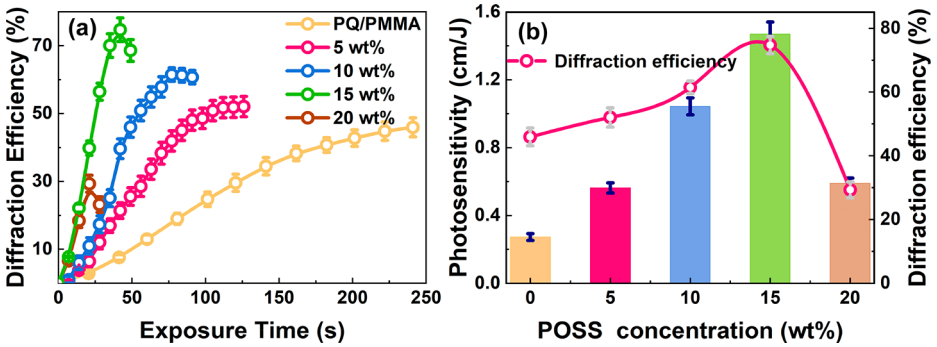

Figure 1. (a) Time-dependent intensity holographic diffraction efficiency about PQ/PMMA and different concentration of POSS−PMMA/PQ polymers. (b) POSS concentration-dependent photosensitivity and diffraction efficiency of POSS−PMMA/PQ.

1.5 mm thickness, and then horizontally placed into an oven at 313 K for 16 h and 333 K for another 4 h to fully conduct thermal polymerization and, at the same time, prevent explosive polymerization. Then, we reduced the temperature of the oven to 313 K for 20 h and 273 K for 2 d to relieve the residual stress. Stirring prepolymerization and a thermal polymerization process applied in the current work effectively promote the polymerization of MMA and POSS to graft PMMA on the POSS matrix, which acted as a base material, thus possessing high mechanical properties and suppressng photoinduced shrinkage during subsequent photopolymerization. Low volume shrinkage during photopolymerization is one of the main indicators and challenges of a photopolymer applied in holographic data storage. For the purposed sample with 1.5 mm thickness, the physical thickness is measured using a micrometer to be 1.50 mm, with an accuracy of 0.002 mm. And the POSS-*g*-PMMA was fabricated via free radical polymerization to analyze the reaction mechanism and structure on the POSS (for gel permeation chromatography (GPC)). POSS (1 wt %) was dispersed in DMF and sonicated 2 h followed by the addition of MMA and AIBN. Then the solution was stirred at 65 °C for 24 h, and the mixture was transferred into centrifuge tubes and centrifuged at the speed of 12 000 rpm for 1 h to collect the bottom solids. This centrifugation was repeated four times. Finally, the collected solid was dried at 60 °C for 24 h.

Holographic Measurements and Recording. The experimental optic setup for intensity holographic diffraction efficiency measurements is illustrated in Figure S2, in which both the reference and signal beam were linearly polarized (s-pol). The green laser (532 nm) with the intensity of 0.127 W/cm^2 was applied in the current study. The temporal diffraction efficiency was recorded per 6 s at the cross-angle of 24°,[66] and the reading time was set to 0.4 s. The diffraction efficiency η is expressed as

$$\eta = \frac{I_{+1}}{I_0 + I_{+1}} \tag{1}$$

where I_{+1} and I_0 represent the intensities of the first-order grating diffraction and the transmitting beams, respectively. The photosensitivity factor S of materials is expressed as

$$S = \frac{1}{Id}\left(\frac{\partial\sqrt{\eta}}{\partial t}\right) \tag{2}$$

where I represents the intensity value of the signal beam (0.127 W cm^{-2}), d is the thickness of photopolymers (1.5 mm), and η is the diffraction efficiency. According to the definition of diffraction efficiency in Kogelnik's coupled wave theory,[67] the grating index modulation Δn of a photopolymer is defined as

$$\Delta n(t) = \frac{\lambda \cos\theta_0}{\pi d} \arcsin\sqrt{\eta} \tag{3}$$

in which λ is the recording information wavelength (532 nm), θ_0 is the internal cross-angle between signal and reference beams (the average refractive index is 1.492 as measured by an Abbe refractometer), d is the thickness of materials (1.5 mm), and η the diffraction efficiency. We note that, due to the coherent depth inside the photopolymers in the current study being evaluated to be ∼12 mm, which is nearly 1 order magnitude thicker than the physical thickness of the photopolymer sample (1.5 mm), the gratings will be fully constructed inside the photopolymer.[37] Meanwhile, the response time[39] τ was calculated as

$$\sqrt{\eta} = \sqrt{\eta_{sat}}[1 - \exp(-t/\tau)] \tag{4}$$

where η_{sat} is the saturation diffraction efficiency.

Characterization. Initially, Fourier transform infrared spectroscopy (FT-IR) was employed to monitor the reaction kinetics induced by the introduction of POSS in thermal- and photopolymerization processes. The polymer matrix prepared by MMA with POSS was used to evaluate the grafting effect in the thermal polymerization procedure. Then, POSS was codissolved in acetone with PQ (1 wt %) and stirred evenly, and the samples with and without beam exposure were dried to achieve the corresponding characterization samples. Finally, PMMA and POSS−PMMA with different mass content (5, 10, 15, and 20 wt %) were prepared to get the information about residual C═C double bond content. FT-IR spectra were performed on a Thermo Nicolet iS5 spectrometer using KBr pellets in the range of 4000−400 cm^{-1} with a resolution of 0.01 cm^{-1}. Raman spectra were characterized by applying an XploRA PLUS Raman microscope with a green laser source of 532 nm 10 mW. Moreover, the sample molecular weights were obtained on a Japan Shimadzu RID-20A system (gel permeation chromatography) equipped with a column at 308 K using THF as the mobile phase and a flow rate of 1 mL min^{-1}.

Furthermore, the samples of POSS with PQ were codissolved in $CDCl_3$ solution. In addition, PQ&POSS were exposed under a green laser with the intensity of 0.127 W cm^{-2} for 24 h to achieve full-exposure samples. ^{13}C NMR spectra for samples, therefore, were characterized for a subsequent micromechanism analysis. We note that tetramethylsilane (TMS) in the current study was introduced as a benchmark. A thermogravimetric analysis (TGA) was performed by using a TGA/DSC1/1100LF in the range of 30−600 °C at a heating rate of 10 °C min^{-1} in N_2 atmosphere, and we used the same conditions to obtain the differential thermogravimetry (DTG) results. In addition, an METASH UV−vis-5200 spectrophotometer was utilized to characterize the absorption spectrum of photopolymers, in which the absorbance (A) was calculated by

$$A = -\ln\frac{I_t}{I_0} \tag{5}$$

where I_0 and I_t are the intensities of the incident and transmitted light, respectively. Moreover, scanning electron microscopy (SEM) images and the distribution of Si element mapping were achieved by utilizing a JEM-2100F electron microscope. SEM samples were prepared by POSS−PMMA/PQ (15 wt %) photopolymer before and after exposure, and the sample was exposed using the intensity holographic diffraction efficiency measurements system, as illustrated in Figure S2. The storage modulus and cure volume shrinkage of POSS−PMMA/

https://doi.org/10.1021/acsami.2c04011
ACS Appl. Mater. Interfaces 2022, 14, 21544−21554

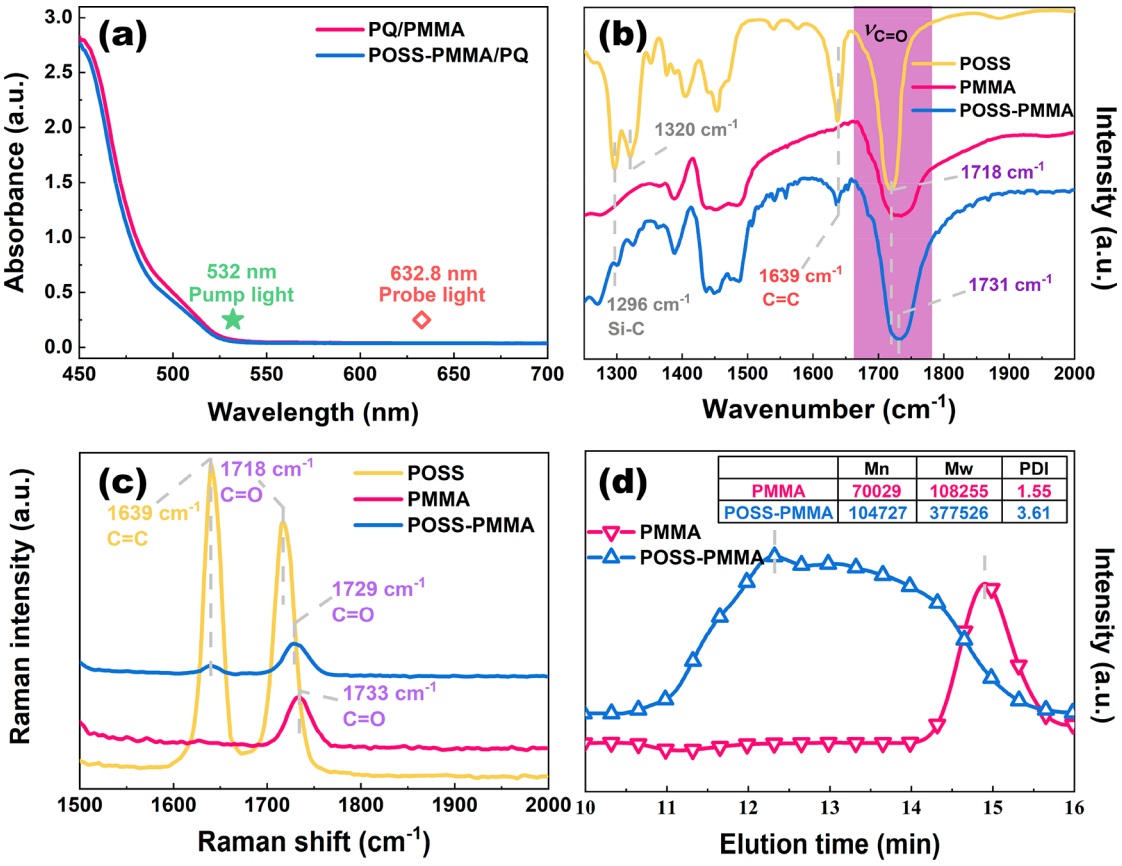

Figure 2. (a) UV−Vis absorption spectra of PQ/PMMA and POSS−PMMA/PQ (15 wt %). (b) FT-IR spectra of POSS, PMMA, and POSS−PMMA (15 wt %). (c) Raman spectra of POSS, PMMA, and POSS−PMMA (15 wt %). (d) GPC evolution curve of PMMA and POSS−PMMA (1 wt %).

PQ materials during photopolymerization were measured using Anton Paar MCR302 rotational rheometer with UV optical accessories in a nitrogen gas atmosphere at 30 °C. The initial thickness, normal stress, angular frequency, and strain were set as 1.0 mm, 0 N, 10 rad/s, and 2%, respectively. Samples were irradiated using a 320−500 nm light source (Omnicure serials 2000) with an intensity of 150 mW/cm^2. The cure volume shrinkage ε[30,68,69] can be calculated by

$$\varepsilon = \left[1 + \frac{1}{3}\left(\frac{h_0 - h_t}{h_0}\right)\right]^3 - 1 \quad (6)$$

where h_0 is the initial gap (1 mm), and h_t is the final gap. Nanoindentation tests were performed using a Nanoindenter Vantage test system, and the hardness and elastic modulus of pristine and POSS−PQ/PMMA materials were characterized before and after s-pol laser exposure (0.127 W cm^{-2} for 30 min). And the value of volume shrinkage σ[29,37,70] of POSS−PMMA/PQ during photopolymerization is calculated by

$$\sigma = 1 - \frac{\tan \theta_{theo}}{\tan \theta_{exp}} \quad (7)$$

in which θ_{theo} and θ_{exp} are the main lobe Bragg angle positions in theory and experiment after two-photon interference in photopolymer. In detail, the main lobe Bragg angles were measured using angle-multiplexing experiments, as illustrated in Figure S2, which were performed by utilizing a computer-controlled motorized Sigma (OSMS-60YAW) stage with a speed of 0.25°/s and a resolution of 0.005° per pulse.

RESULTS AND DISCUSSION

Holographic Performance of Ma-POSS-PMMA/PQ. For traditional intensity holography, in which both signal and reference beam are s-pol, the introduction of POSS can effectively enhance the diffraction efficiency of PQ/PMMA photopolymer, as demonstrated in Figure 1a. The diffraction efficiency can surprisingly reach up to ∼75% as the concentration of POSS is set to be 15 wt %, while it tends to decrease as the POSS concentration continues to increase to 20 wt % due to the dispersion's turbidity increases. The diffraction efficiency of POSS−PMMA/PQ was achieved under low-power laser irradiation conditions in the current study; this efficiency is significantly enhanced by more than 50% as compared to that of PQ/PMMA. Moreover, the grating refractive index modulation (Δn) calculated by Equation 3, as shown in Figure S4, clearly demonstrates that the optimal refractive index modulation can be improved to 1.16×10^{-4} as the POSS concentration is 15 wt %, which is also a milestone breakthrough for PQ/PMMA photopolymers. Not just the diffraction efficiency and refractive index modulation of photopolymers, more importantly, the introduction of POSS also obviously enhances the photosensitivity (S), as illustrated in Figure 1b, in which the photosensitivity (S) of photopolymers with the POSS doping concentration of 15 wt % is ∼5.5 times higher than that of the pristine one (from 0.27 to 1.47 cm J^{-1}). A benefit to the enhancement of the photosensitivity, the response time was also obviously suppressed from ∼75.6 to ∼15.4 s (approximately five

https://doi.org/10.1021/acsami.2c04011
ACS Appl. Mater. Interfaces 2022, 14, 21544−21554

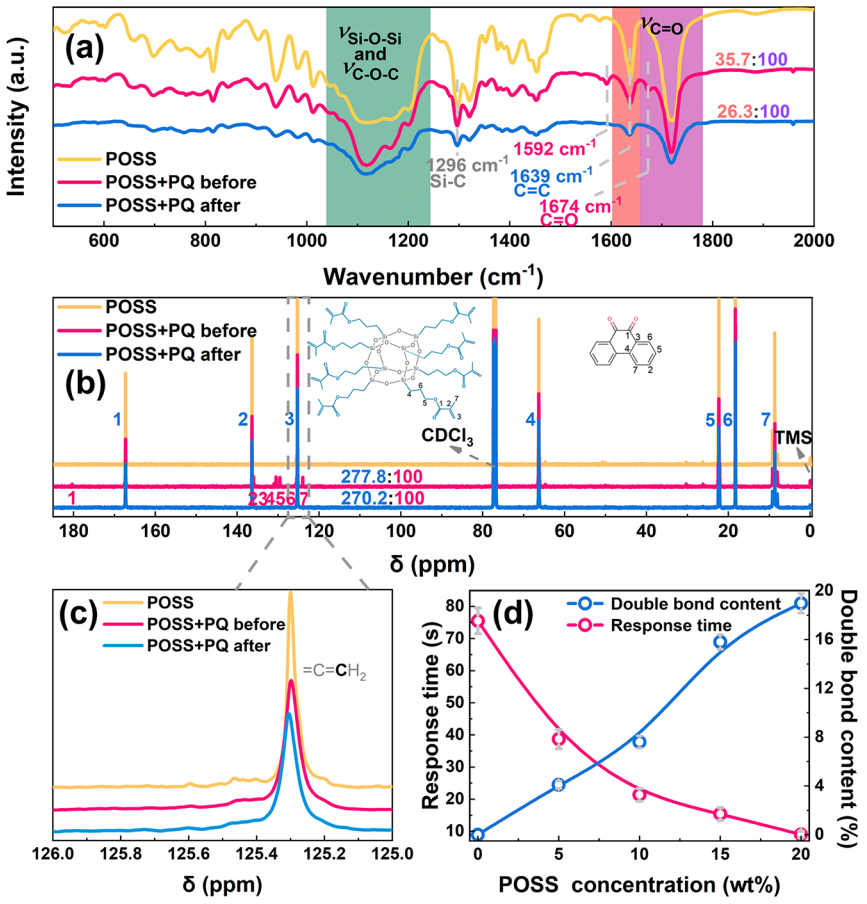

Figure 3. (a) FTIR and (b) ^{13}C NMR spectra of POSS and POSS+PQ matrix before and after exposure. (c) NMR spectra from 125 to 126 ppm. (d) Response time and double bond content with different POSS concentrations in POSS−PMMA/PQ polymers.

times), as illustrated in Figure 3d, which helps speed up holographic data storage effectively.

Microphysical Mechanism of POSS−PMMA/PQ Photopolymers. Taking into account the intrinsic light absorption of POSS, the optical absorption spectra of PQ/PMMA and POSS−PMMA/PQ photopolymers were initially characterized by a UV−vis spectrophotometer. Interestingly, well overlapping the absorption spectrum for photopolymers, as demonstrated in Figure 2a, clearly indicates that the introduction of POSS (15 wt %) in PQ/PMMA photopolymers decreases its light absorption slightly. The lower light absorption coefficient makes the green laser (wavelength of ∼532 nm) more suitable for the pump source to avoid excessive light absorption. Moreover, like a comonomer, Ma-POSS induces the grafting of the PMMA chain on its arms during thermal polymerization. FT-IR spectra, as illustrated in Figure 2b, clearly demonstrate that POSS induces MMA monomers or PMMA polymers grafted on parts of the eight arms. In detail, as compared to the pristine POSS, PMMA, and the characteristic FT-IR transmittance peaks of POSS-doped thermopolymerized PMMA (MMA/AIBN) polymer, the C═C bond in 1639 cm^{-1} dramatically decreased after thermal polymerization, and the C═O bond at 1718 cm^{-1} has a remarkable blue shift to 1731 cm^{-1}. At the same time, lots of FT-IR signals in POSS including the Si−C bond in 1296 cm^{-1} were covered by PMMA polymer chain signals, as marked in Figure S5. Moreover, the Raman spectra as shown in Figure 2c indicate clearly again that, due to the grafting of PMMA onto the C═C bond of POSS, the C═C Raman peak at 1639 cm^{-1} decreased clearly and the C═O bond in 1718 cm^{-1} has a blue shift to 1729 cm^{-1}; at the same time, the C═O bond at 1733 cm^{-1} of PMMA[71] has an obvious red shift to 1729 cm^{-1}. And this Raman shift is very similar to previous star-shaped polymer grafted results about hybrid POSS.[72−74] As illustrated in Figures S6 and S7, because of the very similar structures of the branches of POSS and the PMMA chain, many Raman signals will be covered except the C−C bond at 600 cm^{-1}, the O−H$_3$ bond at 974 cm^{-1}, and the C−H(as) bond at 1455 cm^{-1} after grafting. Furthermore, as demonstrated in Figure 2d, there is an obvious shifted GPC evolution curve, ∼3.5 times the molecular weight (Mw) and 2.5 times the polydispersity index (PDI) of POSS−PMMA compared with PMMA (the maximum weight-average Mw from ∼1.08 × 10^5 to ∼3.77 × 10^5 g/mol, the PDI from 1.55 to 3.61), indicate again that POSS promotes MMA monomer polymerization and induces the grafting behavior of PMMA matrix on parts of its branches to be a star-shaped POSS−PMMA macromolecule. The increase in the PDI means that, with the very different grafting levels of each POSS molecule, some functional groups survive from the thermal polymerization of the POSS−PMMA matrix. And the GPC results of these POSS−PMMA materials (as illustrated in Figure S8) show that both the PDI and Mw have no obvious differences with the increase of the POSS concentration from 5 to 20 wt %.

And then, the residual vinyl on Ma-POSS after thermal polymerization increased the photosensitivity obviously of the POSS−PMMA/PQ matrix. FT-IR spectra clearly indicate that photosensitizer PQ has been consumed totally after a beam

https://doi.org/10.1021/acsami.2c04011
ACS Appl. Mater. Interfaces 2022, 14, 21544−21554

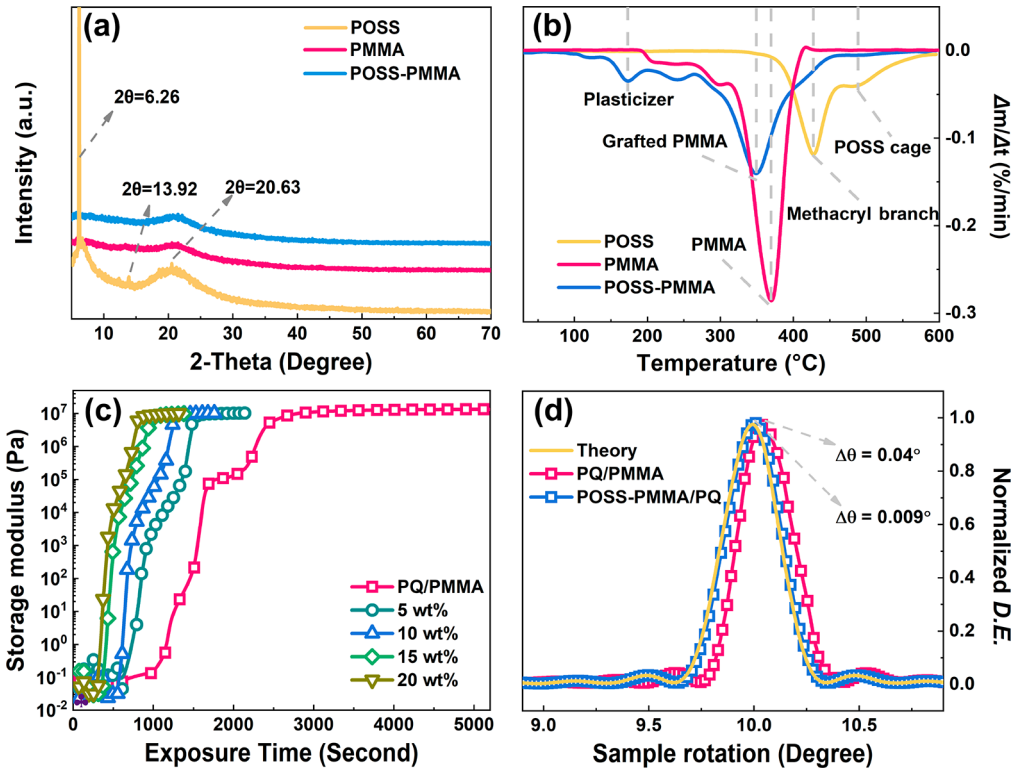

Figure 4. (a) XRD spectra of POSS, PMMA, and POSS−PMMA (15 wt %) materials. (b) DTG results of POSS, PMMA, and POSS−PMMA (15 wt %) materials. (c) Storage modulus results of PQ/PMMA and POSS−PMMA/PQ with different POSS concentrations. (d) Normalized diffraction efficiency of 0.5 mm thick POSS−PMMA/PQ and PQ/PMMA samples that are set to be rotated for 10° from the bisector of two incidence beams as a function of the sample rotation angle.

Table 1. TGA Data of the POSS, PMMA, and POSS−PMMA Materials

sample	Ta_1[a] (°C)	Tb_1[b] (°C)	M_1[c] (%)	Ta_2[a] (°C)	Tb_2[b] (°C)	M_2[c] (%)
POSS	361.47	**427.68**	35.66	467.75	489.57	16.36
PMMA	189.74	**369.43**	97.86			
POSS−PMMA	102.54	173.27	21.34	266.79	**349.29**	45.35

[a]Ta: Initial temperature of degradation. [b]Tb: Temperature at the maximum degradation rate. [c]M: Weight loss percent during the degradation stage.

Table 2. Storage Modulus and Cure Volume Shrinkage of POSS−PMMA/PQ Materials

POSS	0 wt %	5 wt %	10 wt %	15 wt %	20 wt %
Ti[a] (s)	1869.34	912.70	735.04	492.96	368.98
Tf[b] (s)	2807.55	1566.42	1248.38	977.71	781.82
ht[c] (mm)	**0.971**	0.861	0.863	0.865	0.874
Sf[d] (GPa)	0.0134	0.0102	0.0102	0.0099	0.0101
Cs[e] (%)	**2.9**	14.5	14.3	14.1	13.1

[a]Ti: Initial time of cure. [b]Tf: Time to the final cure storage modulus from 100 s (start to exposure). [c]ht: Material's gap of final cure. [d]Sf: Storage modulus of final cure. [e]Cs: Calculated cure volume shrinkage by Equation 6.

exposure in a POSS+PQ (15 wt %) mixture, as shown in Figure 3a. In detail, the C═O bond at 1674 cm^{-1} and the characteristic bond at 1592 cm^{-1} of PQ in POSS+PQ disappeared totally after the beam exposure. At the same time, the double-bond percentage in POSS decreased obviously from 35.7% to 26.3%, where the C═O bond is taken as 100% (C═O will not vary during the thermal- and photopolymerization processes). This phenomenon shows that the photosensitizer PQ will react with the C═C bond of POSS under beam exposure directly. Furthermore, ^{13}C NMR spectroscopy is introduced to deeply investigate the photoreaction between POSS and PQ (before and after exposure) in the deuterated chloroform ($CDCl_3$) solvent; this photoreaction is characterized, as illustrated in Figure 3b,c, where the signal of the four equivalent carbons in TMS is introduced as a benchmark at 0 ppm. The seven ^{13}C characteristic peaks of PQ disappeared after photoreaction with POSS; at the same time, the intensity ratio of peak 3 (═C═$\dot{C}H_2$) to peak 1 (═$\dot{C}$═O) in POSS decreased from 277.3% to 270.2%. At the same time, the characteristic peak of ═C═$\dot{C}H_2$ in POSS has a slight upshift toward the high chemical shift at ∼0.006 ppm (from 125.298 to 125.304 ppm), as shown in Figure 3c. This indicates again that the PQ has a specific photoreaction with the ═C═$\dot{C}H_2$ bond of POSS. Moreover, as illustrated in Figure 3d, the response time calculated by Equation 4 of POSS−PMMA/PQ polymers decreased obviously from ∼75.6 to ∼15.4 s, and the double-bond content increased clearly from 0% to 18.9% with the increase of the POSS concentration from 0 to 20 wt % (double-bond content was calculated from FT-IR spectra in Figure S9). This proved again that the residual vinyl sped up the photoreaction procedure of POSS−PMMA/PQ materials.

Furthermore, X-ray diffraction spectroscopy (XRD) is employed to investigate the polymer structure and dispersible uniformity of POSS in a POSS−PMMA/PQ matrix. As shown in Figure 4a and Figure S10, the pure POSS shows crystalline peaks occur at angles $2\theta \approx 6.26°$, 13.92°, and 20.63°, similar to

https://doi.org/10.1021/acsami.2c04011
ACS Appl. Mater. Interfaces 2022, 14, 21544−21554

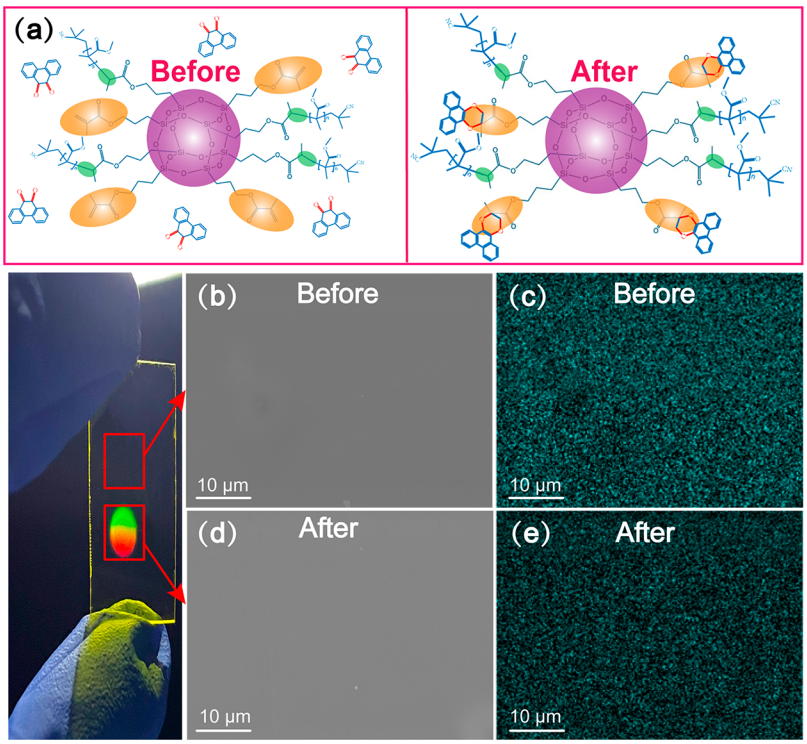

Figure 5. (a) Schematic micromechanism of photoreaction process between the vinyl on POSS and PQ photosensitizers in POSS−PMMA/PQ matrix before and after exposure. SEM images of POSS−PMMA/PQ polymers (b) before and (d) after exposure using two incidence beams; the grating space has a very significant color spot under white light irradiation. Si element energy-mapping results of POSS−PMMA/PQ (c) before and (e) after exposure.

earlier results.[48,75] However, these peaks have vanished in the POSS−PMMA matrix; this demonstrated that the polymerization damaged the POSS crystallization, and it produced the amorphous polymers ascribed to the disordered and random distribution of the POSS units in the whole polymer matrix.[48,76] This proved again that the star-shaped POSS−PMMA polymer was prepared successfully by thermal polymerization. In addition, the TGA and DTG graphs of POSS, PMMA, and POSS−PMMA materials were measured, as illustrated in Figure S11, Figure 4b, and Table 1. The thermal stability of the polymer was closely linked with the decomposition process. DTG results clearly show that the temperature at the maximum degradation rate of POSS, PMMA, and POSS−PMMA were 427.68, 369.43, and 349.29 °C, respectively. The maximum decomposition temperature decreased obviously from 369.43 °C (427.68 °C for POSS) to 349.29 °C, indicating that the PMMA grafted on the methacryl branch of POSS after polymerization. And the star-shaped POSS−PMMA could release the polymer matrix like a plasticizer and then cut down the initial temperature of degradation clearly from 189.74 °C (361.47 °C for POSS) to 102.54 °C. With the continued increase of temperature, the residual methacryls and the central Si−O cages start to degrade at ∼361.47 and ∼467.75 °C, correspondingly. The obvious three-stage decomposition process of POSS−PMMA (first stage from 102.54 to 266.79 °C, second stage from 266.79 to 361.47 °C, and the third stage from 361.47 to 558.80 °C) prove that the PMMA grafted on POSS and, at the same time, that the star-shaped POSS−PMMA can release the polymer matrix as a plasticizer.

In addition, the storage modulus and cure volume shrinkage of POSS−PMMA/PQ materials with different POSS concentrations were measured using a rheometer, as shown in Figure 4c, Figure S12, and Table 2. Both the initial time of cure and the time to the final cure storage modulus from 100 s (start of exposure) were cut down obviously from 1869.34 s (2807.55 s) to 368.98 s (781.82 s) with the increase of the POSS concentration from 0 to 20 wt %, which proves that, with the existence of POSS molecules, the photoreaction of POSS−PMMA/PQ polymers becomes much easier and faster compared with PQ/PMMA. And the final storage modulus of POSS−PMMA/PQ has no big variation. At the same time, the final gap and the cure volume shrinkage of POSS−PMMA/PQ materials were also measured. There is no doubt that the final gap exchange (from 0.139 to 0.126 mm) and the cure volume shrinkage (from 14.5% to 13.1%) decreased with the increase of the POSS concentration from 5 to 20 wt % but increased compared with PQ/PMMA 0.029 mm (2.9%). However, the photoinduced volume shrinkage is much lower than the cure volume shrinkage and has no relationship with it. And we can obviously find that the POSS speeds up the photoreaction process of PQ/PMMA.

The volume shrinkage of photopolymers during holography has an obvious impact on the data storage error rate, and one should pay close attention, because it can result in significant grating distortion, Bragg shifts, and, consequently, the failure of data reading induced by the diffraction decays at the Bragg angle. Then, the photoinduced volume shrinkage of thermal polymerized POSS−PMMA/PQ and PQ/PMMA material was measured, as illustrated in Figure 4d. The photoinduced volume shrinkage can be calculated from the main lobe shift (∼0.009° of POSS−PMMA/PQ and ∼0.04° of PQ/PMMA) using Equation 7, and the POSS suppressed the shrinkage dramatically (over 4 times) from ∼0.4% to ∼0.09% compared

https://doi.org/10.1021/acsami.2c04011
ACS Appl. Mater. Interfaces 2022, 14, 21544−21554

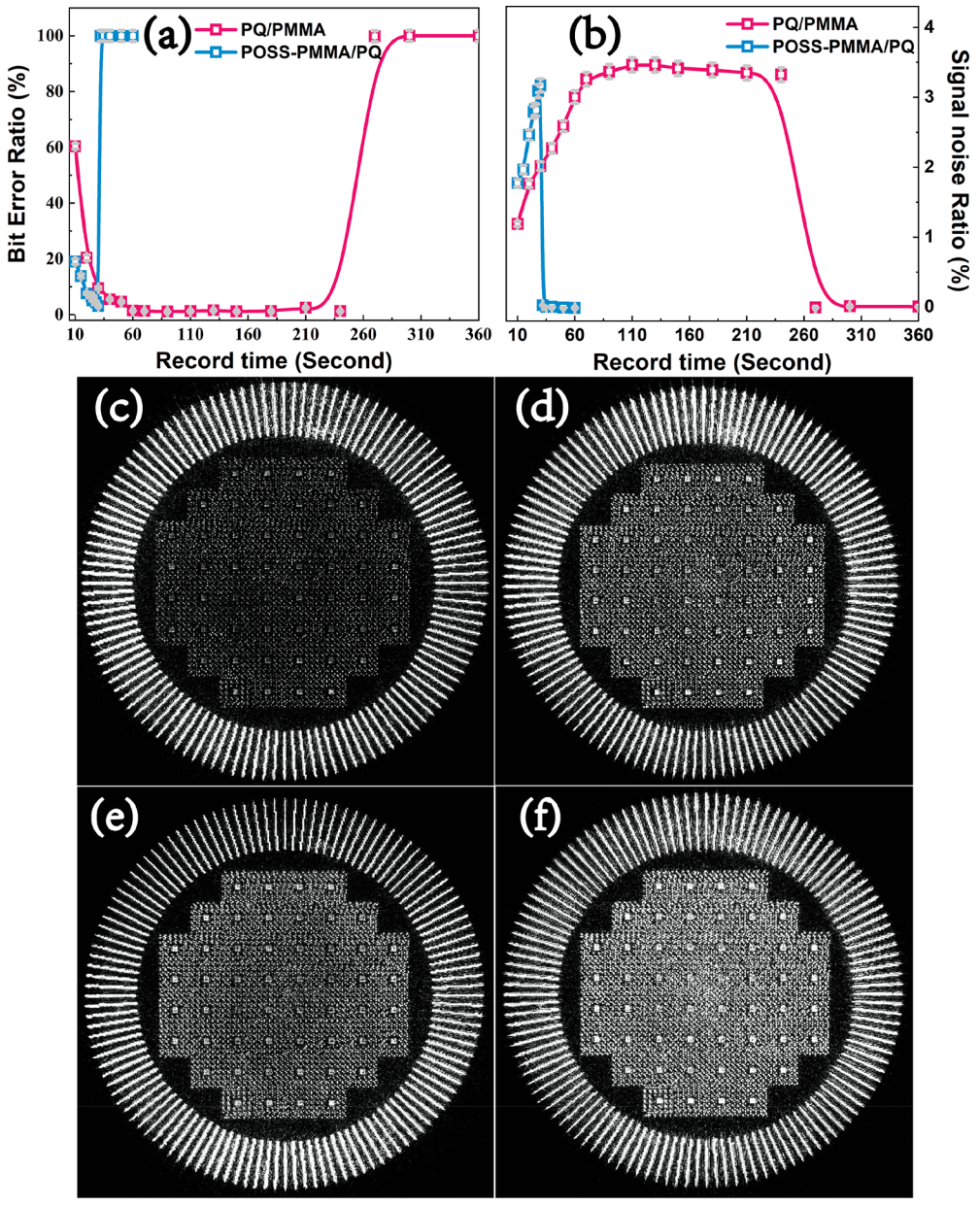

Figure 6. Collinear holographic storage system images: the recording time-dependent BER (a) and SNR (b) results of PQ/PMMA and POSS−PMMA/PQ materials, the read-out images of PQ/PMMA (c) and POSS−PMMA/PQ (d) after exposure for 30 s using a collinear beam, and the overexposed images of PQ/PMMA (e) and POSS−PMMA/PQ (f) polymers after being exposed ∼270 and 35 s, correspondingly.

with PQ/PMMA. The ultralow volume shrinkage of POSS−PMMA/PQ photopolymers should be ascribed to the intrinsic excellent mechanical properties of POSS−PMMA matrix achieved during thermopolymerization, for example, the hardness, elastic modulus, and elastic recovery parameter, which are orders of magnitude higher than PQ/PMMA photopolymers. As illustrated in Table S1 and Figure S13, due to POSS participating in the polymerization process of the PMMA matrix, the observed mechanical properties of POSS−PMMA/PQ are more excellent compared with the pristine PQ/PMMA. In detail, the hardness enhanced from ∼0.15 to 0.20 GPa, the elastic modulus increased from ∼4.0 to 4.8 GPa, and the elastic recovery parameter increased from ∼0.12 to ∼0.15.

The morphology and Si element energy spectrum of POSS−PMMA/PQ polymers were investigated by SEM images, as shown in Figure 5b−e. But both the surface morphology and Si element energy mapping results were not changed before (Figure 5b,c) and after (Figure 5d,e) the exposure, and this phenomenon shows that the POSS molecule has not taken part in the interdiffusion grating formation progress during beam exposure due to the star-shaped POSS−PMMA structures, which is very different from other nanoparticle-doped photopolymers.[77,78] The well-dispersed Si elements indicate that the POSS has no cluster in the POSS−PMMA/PQ matrix, which is in accord very well with the XRD result. And the periodic fringe structure was not found due to the insignificant surface morphology change in the grating spaces. Thence, the experimental investigation mentioned above indicates that microscopic physical mechanisms of POSS on the intensity holographic performance of POSS−PMMA/PQ photopolymers, schematically illustrated in Figure 5a, should be primarily

https://doi.org/10.1021/acsami.2c04011
ACS Appl. Mater. Interfaces 2022, 14, 21544−21554

achieved through the residual double bond on POSS after grafting and the star-shaped POSS−PMMA macromolecular structures.

Collinear Holographic Information Recording of POSS−PMMA/PQ. According to the high sensitivity and ultralow volume shrinkage, POSS−PMMA/PQ photopolymers are also validated in the current study to possess excellent holographic information storage using the collinear holography[24,25] system in our laboratory; the results were illustrated in Figure 6a−f. The record time-dependent BER (Figure 6a) and SNR (Figure 6b) curves show that the POSS−PMMA/PQ material is more sensitive and reliable during information storage and read-out processes compared with PQ/PMMA. And a much lower BER and much higher SNR result, using a short recording time (less than 30 s) by the collinear beam (∼0.146 mW with the beam diameter ∼200 μm); in detail, the BER decreased by ∼70% (from 9.5% to 2.8%), and the SNR increased by ∼57% (from 2.01 to 3.16) with the recording time of 30 s, as illustrated in Figure 6c,d. With recording time going on, the read information images of POSS−PMMA/PQ polymers were overexposed rapidly at 35 s (as shown in Figure 6f), and a much slower process was needed for the overexposure of PQ/PMMA (at 270 s, as shown in Figure 6e). The BER and SNR of the overexposed information figure were set as 100% and 0, correspondingly, in this experiment. The holographic information storage experiment above proved that the POSS−PMMA/PQ material is very suitable for quick holographic information storage.

CONCLUSION

We demonstrated here that, for the first time, the introduction of Ma-POSS in PQ/PMMA photopolymer can effectively enhance holographic properties, in which photosensitivity increased ∼5.5 times, strengthening the holographic diffraction efficiency ∼50% and suppressing the volume shrinkage over 4 times. In addition, the observed photosensitivity of POSS−PMMA/PQ photopolymers (1.47 cm/J) hit a record high under low-power laser irradiation conditions, and ultralow volume shrinkage of ∼0.09% photopolymer was acquired. More importantly, experimental characterizations reveal that the big amount of the residual vinyl on POSS dramatically suppressed the response time of POSS−PMMA/PQ materials. Further analysis shows that the plasticizing effect of star-shaped macromolecular POSS−PMMA loosens the polymer matrix, thence, making the photosensitizer PQ diffusion more effective during beam exposure. A benefit to its intrinsic high photosensitivity, excellent mechanical properties, ultralow volume shrinkage, and the significant enhancement of holographic performance, POSS−PMMA/PQ photopolymer sped up the holographic information storage dramatically using the collinear holography system that we realized, making it a promising medium for fast holographic data storage.

ASSOCIATED CONTENT

Supporting Information

The Supporting Information is available free of charge at https://pubs.acs.org/doi/10.1021/acsami.2c04011.

Schematic of preparation process of POSS−PQ/PMMA; Experimental setup for diffraction efficiency measurement; Collinear holographic storage system; The refractive index modulation of POSS−PMMA/PQ; FT-IR spectra of POSS, PMMA, and POSS−PMMA (15 wt %); Original Raman spectra of POSS, PMMA and the POSS−PMMA polymers; Original Raman spectra of POSS, PMMA, and the POSS−PMMA; GPC evolution curve of PMMA and POSS−PMMA materials; FTIR spectra of PMMA and POSS−PMMA with different POSS concentration; XRD spectra of PMMA and POSS−PMMA; TGA results of POSS, PMMA, and POSS−PMMA; Time evolution gap results of POSS−PMMA/PQ; Nanoindentation loading and unloading curve of PQ/PMMA and POSS-PMMA/PQ before and after exposure; Hardness, elastic modulus, and elastic recovery parameter of PQ/PMMA and POSS−PMMA/PQ (PDF)

AUTHOR INFORMATION

Corresponding Author

Xiaodi Tan − *Information Photonics Research Center, Key Laboratory of Optoelectronic Science and for Medicine of Ministry of Education, Fujian Provincial Key Laboratory of Photonics Technology, Fujian Provincial Engineering Technology Research Center of Photoelectric Sensing Application, Fujian Normal University, Fuzhou 350117, China*; orcid.org/0000-0002-7990-4891; Email: xtan@fjnu.edu.cn

Authors

Po Hu − *College of Photonic and Electronic Engineering, Fujian Normal University, Fuzhou 350117, China; Henan Provincial Key Laboratory of intelligent lighting, Huanghuai University, Zhumadian 463000, China*

Jinhong Li − *College of Photonic and Electronic Engineering, Fujian Normal University, Fuzhou 350117, China*

Junchao Jin − *College of Photonic and Electronic Engineering, Fujian Normal University, Fuzhou 350117, China*

Xiao Lin − *College of Photonic and Electronic Engineering, Fujian Normal University, Fuzhou 350117, China*

Complete contact information is available at: https://pubs.acs.org/10.1021/acsami.2c04011

Notes

The authors declare no competing financial interest.

ACKNOWLEDGMENTS

This work was financially supported by the National Key R & D Program of China (2018YFA0701800); Major Science and Technology Project of Fujian Province (2020HZ01012).

REFERENCES

(1) Reinsel, D.; Gantz, J.; Rydning, J. *The Digitization of the World from Edge to Core*; IDC, 2018; pp 1−26.

(2) Gu, M.; Li, X.; Cao, Y. Optical Storage Arrays: A Perspective for Future Big Data Storage. *Light: Sci. Appl.* **2014**, *3*, e177.

(3) Service, R. F. Nanocrystals May Give Boost to Data Storage. *Science* **2000**, *287*, 1902−1903.

(4) Zhang, J.; Cerkauskaite, A.; Drevinskas, R.; Patel, A.; Beresna, M.; Kazansky, P. G. Eternal 5D Data Storage by Ultrafast Laser Writing in Glass. *Proc. of SPIE* **2016**, 97360U.

(5) Jordan, M. I.; Mitchell, T. M. Machine Learning: Trends, Perspectives, and Prospects. *Science* **2015**, *349*, 255−260.

(6) Butler, K. T.; Davies, D. W.; Cartwright, H.; Isayev, O.; Walsh, A. Machine Learning for Molecular and Materials Science. *Nature* **2018**, *559*, 547−555.

(7) Libbrecht, M. W.; Noble, W. S. Machine Learning Applications in Genetics and Genomics. *Nature Rev. Genet.* **2015**, *16*, 321−332.

(8) Clauset, A.; Larremore, D. B.; Sinatra, R. Data-Driven Predictions in the Science of Science. *Science* **2017**, *355*, 477−480.
(9) Hatfield, P. W.; Gaffney, J. A.; Anderson, G. J.; Ali, S.; Antonelli, L.; Basegmez du Pree, S.; Citrin, J.; Fajardo, M.; Knapp, P.; Kettle, B.; Kustowski, B.; MacDonald, M. J.; Mariscal, D.; Martin, M. E.; Nagayama, T.; Palmer, C. A. J.; Peterson, J. L.; Rose, S.; Ruby, J. J.; Shneider, C.; Streeter, M. J. V.; Trickey, W.; Williams, B. The Data-Driven Future of High-Energy-Density Physics. *Nature* **2021**, *593*, 351−361.
(10) Avila, A. M.; Mezic, I. Data-Driven Analysis and Forecasting of Highway Traffic Dynamics. *Nat. Commun.* **2020**, *11*, 2090.
(11) Gu, M.; Zhang, Q.; Lamon, S. Nanomaterials for Optical Data Storage. *Nature Rev. Mater.* **2016**, *1*, 6070.
(12) Ouyang, X.; Xu, Y.; Xian, M.; Feng, Z.; Zhu, L.; Cao, Y.; Lan, S.; Guan, B.-O.; Qiu, C.-W.; Gu, M.; Li, X. Synthetic Helical Dichroism for Six-Dimensional Optical Orbital Angular Momentum Multiplexing. *Nat. Photonics* **2021**, *15*, 901−907.
(13) Zijlstra, P.; Chon, J. W.; Gu, M. Five-Dimensional Optical Recording Mediated by Surface Plasmons in Gold Nanorods. *Nature* **2009**, *459*, 410−413.
(14) Wu, S.; Duan, S.; Lei, Z.; Su, W.; Zhang, Z.; Wang, K.; Zhang, Q. Supramolecular Bisazopolymers Exhibiting Enhanced Photo-induced Birefringence and Enhanced Stability of Birefringence for Four-Dimensional Optical Recording. *J. Mater. Chem.* **2010**, *20*, 5202−5209.
(15) Li, X.; Lan, T. H.; Tien, C. H.; Gu, M. Three-Dimensional Orientation-Unlimited Polarization Encryption by a Single Optically Configured Vectorial Beam. *Nat. Commun.* **2012**, *3*, 998.
(16) Zhu, L.; Cao, Y.; Chen, Q.; Ouyang, X.; Xu, Y.; Hu, Z.; Qiu, J.; Li, X. Near-Perfect Fidelity Polarization-Encoded Multilayer Optical Data Storage Based on Aligned Gold Nanorods. *Opto-Electronic Adv.* **2021**, *4*, 210002.
(17) Ditlbacher, H.; Krenn, J. R.; Lamprecht, B.; Leitner, A.; Aussenegg, F. R. Spectrally Coded Optical Data Storage by Metal Nanoparticles. *Opt. Lett.* **2000**, *25*, 563−565.
(18) Royon, A.; Bourhis, K.; Bellec, M.; Papon, G.; Bousquet, B.; Deshayes, Y.; Cardinal, T.; Canioni, L. Silver Clusters Embedded in Glass as a Perennial High Capacity Optical Recording Medium. *Adv. Mater.* **2010**, *22*, 5282−5286.
(19) Zhang, J.; Gecevicius, M.; Beresna, M.; Kazansky, P. G. Seemingly Unlimited Lifetime Data Storage in Nanostructured Glass. *Phys. Rev. Lett.* **2014**, *112*, No. 033901.
(20) Langston, J. Project Silica Proof of Concept Stores Warner Bros. 'Superman' Movie on Quartz Glass *Microsoft Innovation Stories*, **2019**.
(21) Yang, Q.; Xie, Z.; Zhang, M.; Ouyang, X.; Xu, Y.; Cao, Y.; Wang, S.; Zhu, L.; Li, X. Ultra-Secure Optical Encryption Based on Tightly Focused Perfect Optical Vortex Beams. *Nanophotonics* **2022**, *11*, 1063−1070.
(22) Heanue, J. F.; Bashaw, M. C.; Hesselink, L. Volume Holographic Storage and Retrieval of Digital Data. *Science* **1994**, *265*, 749−752.
(23) Haw, M. The Light Fantastic. *Nature* **2003**, *422*, 556−558.
(24) Horimai, H.; Tan, X.; Li, J. Collinear Holography. *Appl. Opt.* **2005**, *44*, 2575−2579.
(25) Lin, X.; Liu, J.; Hao, J.; Wang, K.; Zhang, Y.; Li, H.; Horimai, H.; Tan, X. Collinear Holographic Data Storage Technologies. *Opto-Electronic Adv.* **2020**, *3*, 19000401.
(26) Vijayakumar, A.; Katkus, T.; Lundgaard, S.; P Linklater, D.; P Ivanova, E.; Hock Ng, S.; Juodkazis, S. Fresnel Incoherent Correlation Holography with Single Camera Shot. *Opto-Electronic Adv.* **2020**, *3*, 200004.
(27) Lin, S. H.; Hsu, K. Y.; Chen, W.-Z.; Whang, W. T. Phenanthrenequinone-Doped Poly(Methyl Methacrylate) Photopolymer Bulk for Volume Holographic Data Storage. *Opt. Lett.* **2000**, *25*, 451−453.
(28) Chen, Y.; Hu, P.; Huang, Z.; Wang, J.; Song, H.; Chen, X.; Lin, X.; Wu, T.; Tan, X. Significant Enhancement of the Polarization Holographic Performance of Photopolymeric Materials by Introducing Graphene Oxide. *ACS Appl. Mater. Interfaces* **2021**, *13*, 27500−27512.
(29) Peng, H.; Wang, C.; Xi, W.; Kowalski, B. A.; Gong, T.; Xie, X.; Wang, W.; Nair, D. P.; McLeod, R. R.; Bowman, C. N. Facile Image Patterning Via Sequential Thiol-Michael/Thiol-Yne Click Reactions. *Chem. Mater.* **2014**, *26*, 6819−6826.
(30) Ni, M.; Peng, H.; Liao, Y.; Yang, Z.; Xue, Z.; Xie, X. 3D Image Storage in Photopolymer/ZnS Nanocomposites Tailored by "Photo-initibitor. *Macromolecules* **2015**, *48*, 2958−2966.
(31) Alim, M. D.; Glugla, D. J.; Mavila, S.; Wang, C.; Nystrom, P. D.; Sullivan, A. C.; McLeod, R. R.; Bowman, C. N. High Dynamic Range (Deltan) Two-Stage Photopolymers Via Enhanced Solubility of a High Refractive Index Acrylate Writing Monomer. *ACS Appl. Mater. Interfaces* **2018**, *10*, 1217−1224.
(32) Martinez, F. J.; Fernandez, R.; Marquez, A.; Gallego, S.; Alvarez, M. L.; Pascual, I.; Belendez, A. Exploring Binary and Ternary Modulations on a PA-LCOS Device for Holographic Data Storage in a PVA/AA Photopolymer. *Opt. Exp.* **2015**, *23*, 20459−20479.
(33) Day, B. D.; Gu, M.; Smallridge, A. Rewritable 3D Bit Optical Data Storage in a PMMA-Based Photorefractive Polymer. *Adv. Mater.* **2001**, *13*, 1005−1007.
(34) Tomita, Y.; Hata, E.; Momose, K.; Takayama, S.; Liu, X.; Chikama, K.; Klepp, J.; Pruner, C.; Fally, M. Photopolymerizable Nanocomposite Photonic Materials and Their Holographic Applications in Light and Neutron Optics. *J. Mod. Opt.* **2016**, *63*, S1−S3.
(35) Sánchez, C.; Escuti, M. J.; van Heesch, C.; Bastiaansen, C. W. M.; Broer, D. J.; Loos, J.; Nussbaumer, R. TiO_2 Nanoparticle-Photopolymer Composites for Volume Holographic Recording. *Adv. Fun. Mater.* **2005**, *15*, 1623−1629.
(36) Ninjbadgar, T.; Garnweitner, G.; Börger, A.; Goldenberg, L. M.; Sakhno, O. V.; Stumpe, J. Synthesis of Luminescent ZrO_2:Eu^{3+} Nanoparticles and Their Holographic Sub-Micrometer Patterning in Polymer Composites. *Adv. Fun. Mater.* **2009**, *19*, 1819−1825.
(37) Hu, P.; Chen, Y.; Li, J.; Wang, J.; Liu, J.; Wu, T.; Tan, X. Impact of Fullerene on the Holographic Properties of PQ/PMMA Photopolymer. *Comp. Sci. Tec.* **2022**, *221*, 109335.
(38) Li, C.; Cao, L.; Wang, Z.; Jin, G. Hybrid Polarization-Angle Multiplexing for Volume Holography in Gold Nanoparticle-Doped Photopolymer. *Opt. Lett.* **2014**, *39*, 6891−6894.
(39) Liu, P.; Zhao, Y.; Li, Z.; Sun, X. Improvement of Ultrafast Holographic Performance in Silver Nanoprisms Dispersed Photopolymer. *Opt. Exp.* **2018**, *26*, 6993−7004.
(40) Guo, J.; Shi, R.; Wang, R.; Wang, Y.; Zhang, F.; Wang, C.; Chen, H.; Ma, C.; Wang, Z.; Ge, Y.; Song, Y.; Luo, Z.; Fan, D.; Jiang, X.; Xu, J.; Zhang, H. Graphdiyne-Polymer Nanocomposite as a Broadband and Robust Saturable Absorber for Ultrafast Photonics. *Laser Photonics Rev.* **2020**, *14*, 1900367.
(41) Gao, L.; Li, C.; Huang, W.; Mei, S.; Lin, H.; Ou, Q.; Zhang, Y.; Guo, J.; Zhang, F.; Xu, S.; Zhang, H. Mxene/Polymer Membranes: Synthesis, Properties, and Emerging Applications. *Chem. Mater.* **2020**, *32*, 1703−1747.
(42) Guo, J.; Zhao, J.; Huang, D.; Wang, Y.; Zhang, F.; Ge, Y.; Song, Y.; Xing, C.; Fan, D.; Zhang, H. Two-Dimensional Tellurium-Polymer Membrane for Ultrafast Photonics. *Nanoscale* **2019**, *11*, 6235−6242.
(43) Zhang, Y.; Ma, C.; Xie, J.; Agren, H.; Zhang, H. Black Phosphorus/Polymers: Status and Challenges. *Adv. Mater.* **2021**, *33*, No. 2100113.
(44) Kuo, S.-W.; Chang, F.-C. POSS Related Polymer Nanocomposites. *Prog. Polym. Sci.* **2011**, *36*, 1649−1696.
(45) Liu, S.; Guo, R.; Li, C.; Lu, C.; Yang, G.; Wang, F.; Nie, J.; Ma, C.; Gao, M. POSS Hybrid Hydrogels: A Brief Review of Synthesis, Properties and Applications. *Eur. Poly. J.* **2021**, *143*, 110180.
(46) Pyun, J.; Matyjaszewski, K. Synthesis of Nanocomposite Organic/Inorganic Hybrid-Materials Using Controlled-"Living" Radical-Polymerization. *Chem. Mater.* **2001**, *13*, 3436−3448.
(47) Fina, A.; Monticelli, O.; Camino, G. POSS-Based Hybrids by Melt/Reactive Blending. *J.Mater. Chem.* **2010**, *20*, 9297−9305.

https://doi.org/10.1021/acsami.2c04011
ACS Appl. Mater. Interfaces 2022, 14, 21544−21554

(48) Jia, L.; Ma, J.; Gao, D.; Tait, W. R. T.; Sun, L. A Star-Shaped POSS-Containing Polymer for Cleaner Leather Processing. *J. Hazard Mater.* **2019**, *361*, 305−311.
(49) Koehne, I.; Gerstel, M.; Bruhn, C.; Reithmaier, J. P.; Benyoucef, M.; Pietschnig, R. Azido-Functionalized Aromatic Phosphonate Esters in (R)POSS-Cage-Supported Lanthanide Ion (Ln = La, Nd, Dy, Er) Coordination. *Inorg. Chem.* **2021**, *60*, 5297−5309.
(50) Gon, M.; Saotome, S.; Tanaka, K.; Chujo, Y. Paintable Hybrids with Thermally Stable Dual Emission Composed of Tetraphenylethene-Integrated POSS and MEM-PPV for Heat-Resistant White-Light Luminophores. *ACS Appl. Mater. Interfaces* **2021**, *13*, 12483−12490.
(51) Batibay, G. S.; Gunkara, O. T.; Ocal, N.; Arsu, N. Thioxanthone Attached Polyhedral Oligomeric Silsesquioxane (POSS) Nano-Photoinitiator for Preparation of Pmma Hybrid Networks in Air Atmosphere. *Prog. Org. Coat.* **2020**, *149*, 105939.
(52) Doganci, M. D.; Caner, D.; Doganci, E.; Ozkoc, G. Effects of Hetero-Armed Star-Shaped PCL-PLA Polymers with POSS Core on Thermal, Mechanical, and Morphological Properties of PLA. *J. Appl. Polym. Sci.* **2021**, *138*, No. 50712.
(53) Mohamed, M. G.; Kuo, S. W. Functional Silica and Carbon Nanocomposites Based on Polybenzoxazines. *Macr. Chem. Phys.* **2019**, *220*, 1800306.
(54) Ge, Z.; Wang, D.; Zhou, Y.; Liu, H.; Liu, S. Synthesis of Organic/Inorganic Hybrid Quatrefoil-Shaped Star-Cyclic/Polymer Containing a Polyhedral Oligomeric Silsesquioxane Core. *Macromolecules* **2009**, *42*, 2903−2910.
(55) Mohamed, M. G.; Kuo, S. W. Functional Polyimide/Polyhedral Oligomeric Silsesquioxane Nanocomposites. *Polymers* **2019**, *11*, 26.
(56) Lichtenhan, J. D.; Otonari, Y. A.; Carr, M. J. Linear Hybrid Polymer Building Blocks-Methacrylate-Functionalized Polyhedral Oligomeric Silsesquioxane Monomers and Polymers. *Macromolecules* **1995**, *28*, 8435−8437.
(57) Castelvetro, V.; Ciardelli, F.; De Vita, C.; Puppo, A. Hybrid Nanocomposite Films from Mono- and Multi-Functional POSS Copolyacrylates in Miniemulsion. *Macromol. Rapid Commun.* **2006**, *27*, 619−625.
(58) Kuo, S.-W. Hydrogen Bonding Interactions in Polymer/Polyhedral Oligomeric Silsesquioxane Nanomaterials. *J. Poly. Res.* **2022**, *29*, 69 DOI: 10.1007/s10965-021-02885-4.
(59) Pang, B.; Liu, R.; Han, G.; Wang, W.; Zhang, W. The Synthesis of Thermoresponsive POSS-Based Eight-Arm Star Poly(N-Isopropylacrylamide): A Comparison between Z-Raft and R-Raft Strategies. *Poly. Chem.* **2021**, *12*, 2063−2074.
(60) Yao, M. Z.; Liu, Y.; Qin, C. N.; Meng, X. J.; Cheng, B. X.; Zhao, H.; Wang, S. F.; Huang, Z. Q. Facile Fabrication of Hydrophobic Cellulose-Based Organic/Inorganic Nanomaterial Modified with POSS by Plasma Treatment. *Carbohydr. Poly.* **2021**, *253*, 117193.
(61) Bai, J.; Zhang, Y.; Zhang, W.; Ma, X.; Zhu, Y.; Zhao, X.; Fu, Y. Synthesis and Characterization of Molecularly Imprinted Polymer Microspheres Functionalized with POSS. *Appl. Sur. Sci.* **2020**, *511*, 145506.
(62) Kong, Q.; Li, Z.; Ding, F.; Ren, X. Hydrophobic N-Halamine Based POSS Block Copolymer Porous Films with Antibacterial and Resistance of Bacterial Adsorption Performances. *Chem. Engin. J.* **2021**, *410*, 128407.
(63) Mohamed, M. G.; Mansoure, T. H.; Takashi, Y.; Mohamed Samy, M.; Chen, T.; Kuo, S.-W. Ultrastable Porous Organic/Inorganic Polymers Based on Polyhedral Oligomeric Silsesquioxane (POSS) Hybrids Exhibiting High Performance for Thermal Property and Energy Storage. *Micro. Meso. Mater.* **2021**, *328*, 111505.
(64) Shi, H.; Yang, J.; You, M.; Li, Z.; He, C. Polyhedral Oligomeric Silsesquioxanes (POSS)-Based Hybrid Soft Gels: Molecular Design, Material Advantages, and Emerging Applications. *ACS Mater. Lett.* **2020**, *2*, 296−316.
(65) Liu, Y.; Li, Z.; Zang, J.; Wu, A. a.; Wang, J.; Lin, X.; Tan, X.; Barada, D.; Shimura, T.; Kuroda, K. The Optical Polarization Properties of Phenanthrenequinone-Doped Poly(Methyl Methacrylate) Photopolymer Materials for Volume Holographic Storage. *Opt. Rev.* **2015**, *22*, 837−840.
(66) Liu, P.; Sun, X.; Wang, L. Polarization Holographic Characteristics of Ti/PMMA Polymers by Linearly Polarized Exposure. *Opt. Mater.* **2020**, *107*, 109992.
(67) KOGELNIK, H. Coupled Wave Theory for Thick Hologram Gratings. *Bell Syst. Technol. J.* **1969**, *48*, 2909−2947.
(68) Haider, M.; Hubert, P.; Lessard, L. Cure Shrinkage Characterization and Modeling of a Polyester Resin Containing Low Profile Additives. *Compos. Part A-Appl. S.* **2007**, *38*, 994−1009.
(69) Khoun, L.; Hubert, P. Cure Shrinkage Characterization of an Epoxy Resin System by Two in Situ Measurement Methods. *Poly. Comp.* **2010**, *31*, 1603−1610.
(70) Jeong, Y.-C.; Lee, S.; Park, J.-K. Holographic Diffraction Gratings with Enhanced Sensitivity Based on Epoxy-Resin Photopolymers. *Opt. Exp.* **2007**, *15*, 1497−1504.
(71) Thomas, K. J.; Sheeba, M.; Nampoori, V. P. N.; Vallabhan, C. P. G.; Radhakrishnan, P. Raman Spectra of Polymethyl Methacrylate Optical Fibres Excited by a 532 nm Diode Pumped Solid State Laser. *J. Opt. A: Pure Appl. Opt.* **2008**, *10*, 055303.
(72) Xiao, Y.; Tripathy, S.; Lin, T.; He, C. Absorption and Raman Study for POSS-Oligophenylene Nanohybrid Molecules. *J. Nanosci. Nanotechnol.* **2006**, *6*, 3882−3887.
(73) Sulca, N. M.; Lungu, A.; Garea, S. A.; Iovu, H. Monitoring the Synthesis of New Polymer Nanocomposites Based on Different Polyhedral Oligomeric Silsesquioxanes Using Raman Spectroscopy. *J. Raman Spectrosc.* **2009**, *40*, 1634−1640.
(74) Weng, J. T.; Yeh, T. F.; Samuel, A. Z.; Huang, Y. F.; Sie, J. H.; Wu, K. Y.; Peng, C. H.; Hamaguchi, H. O.; Wang, C. L. Cylindrical Micelles of a POSS Amphiphilic Dendrimer as Nano-Reactors for Polymerization. *Nanoscale* **2018**, *10*, 3509−3517.
(75) Leu, C. M.; Chang, Y. T.; Wei, K. H. Polyimide-Side-Chain Tethered Polyhedral Oligomeric Silsesquioxane Nanocomposites for Low-Dielectric Film Applications. *Chem. Mater.* **2003**, *15*, 3721−3727.
(76) Li, D.; Niu, Y.; Yang, Y.; Wang, X.; Yang, F.; Shen, H.; Wu, D. Synthesis and Self-Assembly Behavior of Poss-Embedded Hyperbranched Polymers. *Chem. Commun.* **2015**, *51*, 8296−8299.
(77) Schuller, J. A.; Tomita, Y.; Urano, H.; Fukamizu, T.-a.; Kametani, Y.; Nishimura, N.; Odi, K. Photopolymerizable Polymer Nanocomposites Incorporated with Hyperbranched Polymer Having Ultrahigh Index of Refraction for Holographic Light Manipulation. In *Light Manipulating Organic Materials and Devices II*; SPIE, 2015; Vol. *9564*. DOI: 10.1117/12.2187747.
(78) Tomita, Y.; Hata, E.; Momose, K.; Takayama, S.; Liu, X.; Chikama, K.; Klepp, J.; Pruner, C.; Fally, M. Photopolymerizable Nanocomposite Photonic Materials and Their Holographic Applications in Light and Neutron Optics. *J. Mod. Opt.* **2016**, *63*, S1−S31.